



Nanoscale

**Electric Field Tuned Anisotropic to Isotropic Thermal  
Transport Transition in Monolayer Borophene Without  
Alternating Atomic Structures**

Journal:	<i>Nanoscale</i>
Manuscript ID	NR-ART-04-2020-003273.R1
Article Type:	Paper
Date Submitted by the Author:	01-Aug-2020
Complete List of Authors:	Yang, Zhonghua; Shenyang University of Technology Yuan, Kunpeng; Dalian University of Technology, Meng, Jin; Shenyang University of Technology Hu, Ming; University of South Carolina, Mechanical Engineering

SCHOLARONE™  
Manuscripts

# Electric Field Tuned Anisotropic to Isotropic Thermal Transport Transition in Monolayer Borophene Without Alternating Atomic Structures

Zhonghua Yang<sup>1,2,#</sup>, Kunpeng Yuan<sup>2,3,#</sup>, Jin Meng<sup>1</sup>, and Ming Hu<sup>2,\*</sup>

<sup>1</sup>*College of Architecture and Civil engineering, Shenyang University of Technology, Shenyang, 110870, China*

<sup>2</sup>*Department of Mechanical Engineering, University of South Carolina, Columbia, 29208, USA*

<sup>3</sup>*Key Laboratory of Ocean Energy Utilization and Energy Conservation of Ministry of Education, School of Energy and Power Engineering, Dalian University of Technology, Dalian 116024, China*

## Abstract

Thermal anisotropy/isotropy is one of fundamental thermal transport properties of materials and plays a critical role in a wide range of practical applications. Manipulation of anisotropic to isotropic thermal transport or vice versa is in increasing demand. However, almost all the existing approaches for tuning anisotropy or isotropy focus on structure engineering or materials processing, which is time and cost consuming and irreversible, while little progress has been made with intact, robust, and reversible method. Motivated by the inherent relationship between the interatomic interaction mediated phonon transport and the electronic charges, we comprehensively investigate the effect of external electric field on the thermal transport in two-dimensional (2D) borophene, by performing first-principles calculations along with the phonon Boltzmann transport equation. Under external electric field, the lattice thermal conductivity of borophene in both in-plane directions first increases significantly to the peak values with maximum augmentation factor of 2.82, and the intrinsic anisotropy (the ratio of thermal conductivity along two in-plane directions) is boosted to the highest value of 2.13. After that, thermal conductivities drop down steeply and the anisotropy exhibits oscillating decay. With electric field increasing to  $0.4 \text{ V}/\text{\AA}$ , the thermal conductivity is dramatically suppressed to 1/40 of the original value at no electric field. More interestingly, the anisotropy of the thermal conductivity decreases to the minimum value of 1.25, showing almost

---

<sup>#</sup>These authors contributed equally to this work.

<sup>\*</sup> Author to whom all correspondence should be addressed. E-Mail: [hu@sc.edu](mailto:hu@sc.edu) (M.H.)

isotropic thermal transport. Such abnormal anisotropic to isotropic thermal transport transition stems from the large enhancement and suppression of phonon lifetime at moderate and high strength of electric field, respectively, which acts as amplifying or reducing factor to the thermal conductivity. We further explain the tunability of phonon lifetime of the dominant acoustic mode by the electron localization function. By comparing the electric field-modulated thermal conductivity of borophene with the dielectric constant, it is found that the screened potential resulting from the redistributed charge density leads to phonon renormalization and the modulation of phonon anharmonicity and anisotropy through electric field. Our study paves the way for robustly tuning anisotropy of phonon transport in materials by intact, robust, and reversible external electric field without altering the atomic structure, and would have a significant impact on emerging applications, such as thermal management of nanoelectronics and thermoelectric energy conversion.

**Keywords:** Thermal Transport; Anisotropy; Borophene; Two-Dimensional Materials; First-Principles

## 1 Introduction

Heat transfer is one of the main forms of energy transfer in nature. Efficiently manipulating thermal transport in materials is one of the most appealing fundamental thermal physical problems, with two representatives but opposing aspects: on the one hand, increasing the thermal conductivity of the material to eliminate the heat accumulated performance of electronic equipment is essential to extend its life; on the other hand, reducing the thermal conductivity of the material is significant in the thermoelectricity and thermal insulation field. In order to expand the application of new materials more widely, tremendous amounts of research efforts have been dedicated in the past years to exploring robust ways to effectively modulate thermal transport. While almost all the existing approaches for tuning thermal conductivity focus on structure engineering or materials processing, the robust and reversible method by external electric field receives less attention.

Borophene is a close relative of graphene and has been predicted for more than 10 years. Experimentally, the quasi-planar  $B_{35}$  and  $B_{36}$  clusters with hexagonal vacancies were observed before, and they are viewed as a potential basis for extended 2D boron sheets<sup>1</sup>. However, unlike the great success of carbon materials, boron materials have received relatively less attention due to the huge challenges in experimental implementation. Until December 2015, borophene has been grown successfully on single crystal Ag (111) substrates under ultrahigh-vacuum conditions and since then it attracted tremendous research interests due to its extraordinary physical and chemical properties<sup>2</sup>. Especially, thermal transport in different phases of borophene has become an attractive topic<sup>3-4-5-6-7</sup>. The anisotropic thermal transport and moderate thermal conductivity make borophene promising in applications of transparent conductor and thermal management<sup>8</sup>. Zhou<sup>9-10</sup> et al. pointed out that the high frequency phonons of the borophene all travel in one direction, resulting in their high thermal conductivity. The anomalous behavior is further explained by the electron density distribution which indicates that the electron density of borophene is highly anisotropic. Similarly, molecular dynamics simulation is performed by Mortazavi et al. to illustrate that the anisotropy of borophene thermal conductivity is attributed to differences in the density of states of low-frequency range, which correlate to lower group velocities and possibly shorten phonon lifetimes along the zigzag direction<sup>11</sup>. The stability of anisotropy in borophene nanoribbons depends on the large-scale localization of electrons

along boron rows. The linear boundary borophene thins form extra  $\pi$  bonds by reconstructing the edges to stabilize the electron-deficient edge atoms<sup>12</sup>. Xiao et al. used borophene instead of  $\alpha'$ -boron sheet and the lattice thermal conductivity of borophene is gained by the first-principles calculation. The value is 14.34  $\text{Wm}^{-1}\text{K}^{-1}$  at room temperature along the armchair, which is substantially smaller than that of graphene<sup>13</sup>. Gao<sup>14</sup> et al. confirmed that electron-phonon coupling constants in the two compounds are larger than that in  $\text{MgB}_2$ . The superconducting transition temperatures were determined to be 18.7 K and 24.7 K through the McMillian-Allen-Dynes formula. Xiao<sup>15</sup> et al. further showed that the superconductivity of borophene can be significantly enhanced by strain and charge carrier doping. The tensile strain can increase the transition temperature to 27.4 K, while the hole doping can notably increase the transition temperatures to 34.8 K. The superior mechanical flexibility of borophene along the  $\vec{b}$  direction was investigated through valence charge density. It was found that the bonds of  $\text{B}_1\text{-B}_2$  in the intermediate layer are weakened with the increase of the  $b$ -axis strain, which causes an out-of-plane negative Poisson's ratio<sup>16</sup>. Wang<sup>4</sup> et al. further explained that the pristine borophene has significant in-plane Young's moduli and Poisson's ratio anisotropy due to its strong and highly coordinated B-B bonds.

It is not difficult to find from previous research results that the force-electricity-heat of borophene is inseparable from the electrostatic interactions. Based on this premise, we propose an idea to apply an external electric field to affect the interatomic electrostatic interaction, and finally alter the thermal conductivity. In this paper, we demonstrate that the thermal conductivity of borophene, in particular the anisotropy of thermal transport in two different directions, is very sensitive to a vertical external electric field. Fundamental insight into the electric field-modulated lattice thermal conductivity and the anisotropy of the in-plane thermal transport are gained by analyzing the phonon anharmonicity from the microscopic view of the phonon parameters and electronic structure. Our study provides solid evidence for robustly modulating phonon transport in low-dimensional materials by applying external electric field, which is expected to have broad impact on lots of applications, such as thermal management of nanoelectronics and thermoelectrics.

## 2 Computational Model and Methods

All the calculations are based on density functional theory (DFT) as implemented in the Vienna ab initio simulation package (VASP)<sup>17-18-19</sup>. The Perdew-Burke-Ernzerhof (PBE)<sup>20</sup> of the generalized gradient approximation (GGA) is chosen as the exchange-correlation functional. The kinetic energy cutoff of the wave functions is set as 450 eV, and a Monkhorst-Pack<sup>21</sup> k-mesh of  $27 \times 15 \times 1$  is used to sample the Brillouin Zone (BZ). The lattice constants and internal coordinates are optimized until the atomic forces become less than  $10^{-4}$  eV/Å. A large vacuum spacing of 20 Å is employed along the out-of-plane direction to eliminate the interaction between periodic images. To simulate a perpendicular electric field, VASP introduces dipole sheets in the middle of the vacuum regions, the electric field along the out-of-plane direction is applied and the dipole corrections are considered<sup>22</sup>.

It is well-known that the thermal conductivity is governed by the specific heat capacity, group velocity, and phonon lifetime :

$$\kappa_{\alpha} = \sum_{\lambda} c_{ph,\lambda} v_{\alpha,\lambda}^2 \tau_{\lambda} \quad (1)$$

where  $\kappa_{\alpha}$  denotes the lattice thermal conductivity in  $\alpha$  direction,  $\lambda$  represents a phonon mode with wave vector  $\mathbf{q}$  and phonon branch  $\mathbf{s}$ ,  $v_{\alpha,\lambda}$  is the phonon group velocity of mode  $\lambda$  along  $\alpha$  direction,  $\tau_{\lambda}$  is the phonon lifetime of mode  $\lambda$ , and  $c_{ph}$  refers to the phonon volumetric specific heat of each mode

$$c_{ph} = \frac{k_B}{NV} \frac{(\hbar\omega_{\lambda} / k_B T^2) e^{\hbar\omega_{\lambda} / k_B T}}{(e^{\hbar\omega_{\lambda} / k_B T} - 1)^2} \quad (2)$$

where  $k_B$  is the Boltzmann constant,  $N$  is the  $\mathbf{q}$  points number in the first Brillouin zone,  $V$  is the unite cell volume,  $\hbar$  is reduced Planck constant,  $T$  is the absolute temperature,  $\omega$  is the phonon angular frequency of mode  $\lambda$ . The group velocity of phonon mode  $\lambda$  is the gradient of frequency concerning reciprocal space coordinates:

$$v_{\lambda} = \nabla_{\mathbf{q}} \omega_{\lambda} \quad (3)$$

The phonon lifetime is one of the key input parameters determining the lattice thermal conductivity. The finite lifetime of a specific phonon mode depends on various scattering mechanisms, such as the intrinsic

phonon-phonon scattering, the phonon-isotope scattering, and the phonon-boundary scattering. The total phonon lifetime is expressed by Matthiessen's rule as:

$$\frac{1}{\tau_{\lambda}} = \frac{1}{\tau_{\lambda}^{anh}} + \frac{1}{\tau_{\lambda}^{iso}} + \frac{1}{\tau_{\lambda}^B} \quad (4)$$

where  $\tau_{\lambda}^{anh}$ ,  $\tau_{\lambda}^{iso}$ ,  $\tau_{\lambda}^B$  are the intrinsic phonon-phonon scattering rates, phonon-isotope scattering rates, and the phonon-boundary scattering rates, respectively.

Specifically, the lattice thermal conductivity ( $\kappa_l$ ) is obtained by iteratively solving the linearized Boltzmann-Peierls transport equation as implemented in the ShengBTE package<sup>23</sup> which requires the inputs of second-order harmonic and third-order anharmonic interatomic force constants (IFCs). A  $7 \times 5 \times 1$  supercell and a  $\Gamma$ -centered  $7 \times 5 \times 1$  k-mesh are chosen to calculate the harmonic and anharmonic IFCs. The second-order harmonic IFCs are used to determine the phonon frequency and phonon eigenvector using the Phonopy code<sup>24</sup>. A script of `thirdorder.py` is used to obtain the third-order IFCs which can be evaluated based on the third-order derivatives of the total energy with respect to the atomic displacements. This program predicts the material's  $\kappa_l$  without any other adjustable parameters except the basic information of the chemical structure.

### 3 Simulation Result and Discussion

#### 3.1 Electric field modulated geometry structure and system energy

The optimized structure of borophene is illustrated in Figure 1 which shows the typical monolayer structure. Both optimized lattice constants  $a = 2.871 \text{ \AA}$ ,  $b = 1.617 \text{ \AA}$  are consistent with previous theoretical calculations<sup>25-10</sup>. In this structure, the shortest B-B bond length is  $1.617 \text{ \AA}$ , which is  $0.251 \text{ \AA}$  shorter than the longest length, indicating that the strength of B-B chemical bond is different along different directions. Two planes of rectangular lattice form a buckled structure, with a buckling distance of  $0.88 \text{ \AA}$ . By adding the diameter of boron atom of  $1.81 \text{ \AA}$ , the thickness of borophene is chosen as  $2.69 \text{ \AA}$ . The electric field is applied along the downward (out-of-plane) direction as indicated by the arrow in Figure 1(b).

The lattice constant and buckling distance changes with the strength of external electric field, as shown in Figure 2. It can be seen in Figure 2(a) that, as the electric field increases, the dipole moment increases linearly. In Figure 2(b), both the lattice constant and buckling distance do not have noticeable change until the strength of the external electric field exceeds  $0.04 \text{ V}/\text{\AA}$ . After that, all structural parameters increase in an exponential form with electric field and the buckling distance increases even faster. At electric field of  $0.2 \text{ V}/\text{\AA}$ , the lattice constant and buckling distance are only increased by 0.34% and 0.72%, respectively. Thus, the buckled structure of borophene still holds stably. Further, with the strength of the electric field increasing, the total energy of the borophene supercell decreases, showing a more thermodynamically stable structure in the external electric field, which is the basis for further phonon transport calculation.

### 3.2 Electric field tuned lattice thermal conductivity and anisotropy of thermal transport

In the condition of considering the phonon-phonon scattering as determined by phonon anharmonicity, the lattice thermal conductivity ( $\kappa_l$ ) of borophene is obtained by solving the phonon BTE. The thermal conductivity convergence of borophene with respect to the cutoff radius and  $Q$ -grid are fully examined in Figure 3. The convergence of cutoff radius of anharmonic IFCs should be tested firstly, because the cutoff radius can be directly determined to get satisfactory thermal conductivity results based on the analysis of harmonic IFCs<sup>26</sup>. In order to quantify the strength of interatomic interactions which are described by harmonic IFCs, we calculated the normalized trace of interatomic force constant tensors<sup>27</sup>. According to this parameter, one can directly determine how large the cutoff radius should be to evaluate the anharmonic IFCs by effectively including the possibly strong interaction strength as revealed by the large trace value. Figure 3(a) is the normalized trace of IFC in borophene, it is clear that there exists strong interactions between boron atoms when the cutoff radius is less than 0.4 nm (seventh-nearest neighbors). When the threshold of cutoff radius is bigger than 0.4 nm, the trace values are very weak, indicating negligible force constants. Similar conclusions can also be obtained by the convergence test of borophene thermal conductivity in Figure 3(b). Before the cutoff radius achieving the threshold of 0.4 nm, the borophene thermal conductivities along  $\vec{a}$ ,  $\vec{b}$  directions drop dramatically, and the thermal conductivity converges quickly up to the seventh-nearest neighbors, which confirm the evaluation from the strength of the harmonic

IFCs in Figure 3(a). It is also shown in Figure 3(c) that the thermal conductivity of borophene possesses a well-converged behavior when the  $Q$ -grid is greater than  $33 \times 59 \times 1$ . Therefore, considering both computational cost and accuracy, the interactions are truncated up to the seventh-nearest neighbors and  $Q$ -grid is set as  $33 \times 59 \times 1$  for the following anharmonic IFCs calculations.

Base on the converge test of anharmonic IFCs, the temperature dependent lattice thermal conductivity of borophene is shown in Figure 4(a). The thermal conductivity of borophene with no electric field is remarkably anisotropic and unexpectedly low. Within the considered temperature range, for both in-plane directions [see definition in Figure 1] the thermal conductivities of borophene decrease with temperature increasing. At room temperature, the thermal conductivities of borophene along  $\vec{a}$ ,  $\vec{b}$  directions are  $39.61 \text{ Wm}^{-1}\text{K}^{-1}$  and  $73.48 \text{ Wm}^{-1}\text{K}^{-1}$ , respectively, which are significantly lower than that of graphene<sup>26</sup>. The thermal conductivity along the  $\vec{b}$  direction is around 1.85 times that along the  $\vec{a}$  direction. These results agree very well with previous study<sup>28</sup>. Furthermore, the cumulative thermal conductivity with respect to the phonon mean free path ( $\lambda$ ) at 300 K is plotted in Figure 4(b), which is helpful for the study of size effect on the ballistic or diffusive phonon transport. The cumulative thermal conductivities of borophene along  $\vec{a}$ ,  $\vec{b}$  directions keep increasing as  $\lambda$  increases, and then approaches a plateau after  $\lambda$  reaches 100 nm. It means that the  $\lambda$  is critical to affect the thermal conductivity of borophene when the nanostructure size below the characteristic size<sup>29</sup>. To better understand the reason of anisotropic thermal conductivity, we compare the phonon group velocity of borophene along two in-plane directions [Figure 4(c)]. The maximum value of group velocity is  $21.845 \text{ km/s}$  which is similar to previous research results<sup>28</sup> ( $21.8 \text{ km/s}$ ) and that of graphene ( $21.9 \text{ km/s}$ ). Moreover, it is clearly seen that generally the phonon group velocities along  $\vec{b}$  direction are remarkably higher than that along  $\vec{a}$  direction, which is primarily responsible for the anisotropic thermal conductivity as found in Figure 4(a).

Next, when the external electric field is switched on, the thermal conductivities of borophene along  $\vec{a}$  and  $\vec{b}$  directions first increase until electric field reaches  $0.04 \text{ V/\AA}$  and then drops down steeply until electric fields reach  $0.4 \text{ V/\AA}$  [see Figure 5(a)]. However, the increase and decrease rate of thermal conductivity along  $\vec{a}$  and  $\vec{b}$  directions are different, which leads to a tremendous change in the anisotropy of the thermal transport in these directions, as we will discuss below. The maximum thermal conductivity values

of borophene are  $97.41 \text{ Wm}^{-1}\text{K}^{-1}$  and  $207.25 \text{ Wm}^{-1}\text{K}^{-1}$  along  $\vec{a}$  and  $\vec{b}$  directions, respectively. The peak values at the electric field of  $0.04 \text{ V}/\text{\AA}$  are 2.46 and 2.82 times of the thermal conductivities without external electric field, respectively. The lowest thermal conductivity values of borophene at the largest electric field of  $0.4 \text{ V}/\text{\AA}$  are  $1.48 \text{ Wm}^{-1}\text{K}^{-1}$  and  $1.85 \text{ Wm}^{-1}\text{K}^{-1}$  along  $\vec{a}$  and  $\vec{b}$  directions, respectively, which are only 3.74% and 2.52% of their respective thermal conductivities without external electric field. These results indicate that the external electric field can robustly modulate the phonon transport in 2D borophene. A quick evaluation of frequency resolved thermal conductivity as presented in Figure 5(b) implies that the phonon transport in monolayer borophene with or without external electric field is always dominated by the phonon modes with frequency of 7.5-10 THz, which is exactly the region of acoustic phonons [see Figure 7 below]. In this frequency range, the phonon contribution to overall heat conduction in borophene is 53%, 78%, and 50% for the electric field of  $0 \text{ V}/\text{\AA}$ ,  $0.04 \text{ V}/\text{\AA}$ , and  $0.2 \text{ V}/\text{\AA}$ , respectively. This result is important for our further discussion and analysis below.

More interestingly, the anisotropy of thermal conductivity of monolayer borophene can be dramatically tuned with different strengths of external electric field [see Figure 6]. At electric field of  $0.04 \text{ V}/\text{\AA}$  the ratio of thermal conductivity along  $\vec{b}$  direction to  $\vec{a}$  direction increases from 1.86 to 2.13 (by 15%). As electric field increases further, the anisotropy of thermal conductivity of monolayer borophene exhibits an oscillating behavior. The lowest ratio of thermal conductivity along  $\vec{b}$  direction to  $\vec{a}$  direction reaches 1.25 at electric field of  $0.4 \text{ V}/\text{\AA}$ .

Before we analyze the detailed mechanism of the strong dependence of anisotropy of thermal transport in borophene, we first need to exclude an intuitive factor of the small structure change [see Figure 2(b)], i.e. whether the thermal conductivity change is induced by the tiny atom structure change or by the external electric field? To answer this question, herein we perform a computer experiment. We use the same optimized atomic structure under each different electric field and re-calculate the second-order harmonic and third-order anharmonic interatomic force constants without electric field switched on and finally re-calculate the thermal conductivity. In this way, the obtained thermal conductivity is solely the effect of electric field, not the structure change. From the inset of Figure 5(a), there is little variation in the thermal conductivity, which directly proves that the external electric field is indeed critical for the strong

dependence of anisotropy of thermal transport in borophene as identified in Figure 6.

### 3.3 Phonon dispersion of monolayer borophene

Phonon dispersion is crucial for the calculation of phonon transport properties. By using finite displacement difference (FDD) method, we obtained the IFCs and hence the phonon dispersion relation of borophene [see Figure 7]. The high symmetry path of monolayer borophene is  $\Gamma$ -X-S-Y- $\Gamma$ . The unit cell of borophene contains two atoms, resulting in six dispersion branches. The longitudinal acoustic (LA) and transverse acoustic (TA) branches correspond to vibration within the plane, and the other one (ZA) corresponds to out of plane vibration. Mainly attributed to the intrinsic buckled geometric, three-acoustic branches of borophene present linear dispersion versus the wave vector around the  $\Gamma$  point, which is similar to the silicene and phosphorene<sup>30-31</sup>. However, this behavior is different from ZA branch of graphene, which has a quadratic dispersion around  $\Gamma$  point<sup>32</sup>. It is worth mentioning that the ZA branch of borophene has a small imaginary frequency near  $\Gamma$  point, which indicates that the lattice may exhibit instability<sup>2</sup>. But the structure may be stable when supported by a proper substrate, and such small imaginary should not significantly affect the thermal conductivity calculations, the same as previous study<sup>9</sup>. The average acoustic Debye temperature can be derived from<sup>33</sup>:

$$\frac{1}{\theta_D^3} = \frac{1}{3} \left( \frac{1}{\theta_{ZA}^3} + \frac{1}{\theta_{TA}^3} + \frac{1}{\theta_{LA}^3} \right) \quad (5)$$

where  $\theta_i$  is obtained by  $\theta_i = \hbar \omega_{i,\max} / k_B$ ,  $i$  is each acoustic branch (ZA, TA, LA).  $\omega_{i,\max}$  is maximum of each phonon frequency at the zone boundary. The calculated average acoustic Debye temperature for borophene is 648 K, which is higher than that of monolayer MoS<sub>2</sub> (262.3 K)<sup>31</sup> and black phosphorene (500 K)<sup>34</sup>, but lower than that of graphene (2300 K)<sup>35</sup>. The higher Debye temperature indicates that borophene possesses a strong interatomic bonding.

Comparing phonon dispersions under different electric fields, we found that the phonon dispersions of borophene change very slightly. According to Eq. (3), the phonon group velocity is given by the slope of the dispersion relation. Due to the consistency of the phonon dispersion, the group velocity has no big change with different electric fields. However, the phonon dispersions of the acoustic modes along the  $\vec{a}$

direction are generally much flatter than that along the  $\vec{b}$  direction. Such phenomenon implies that the phonon group velocity in  $\vec{a}$  direction is smaller than that in  $\vec{b}$  direction, which is the result in Figure 4(c). As previously analyzed, due to the anisotropy of the borophene structure itself, the phonon group velocities in  $\vec{a}$  and  $\vec{b}$  directions are different. The analysis of Figure 2(b) and Figure 7 above shows that, (1) the influence of electric fields on borophene structure is small; (2) the influence of the structural change on the thermal conductivity is negligible; and (3) the structural change is not reflected in the phonon spectrum. Therefore, in order to find the root reason of the drastic increase and decrease in the thermal conductivity of borophene at the electric fields of  $0.04 \text{ V/\AA}$  and  $0.4 \text{ V/\AA}$ , we need to explain from the perspective of phonon lifetime, which is another dominant factor of thermal conductivity.

### 3.4 Phonon lifetime and anharmonicity

We present the frequency dependent phonon lifetime for some representative electric fields in Figure 8. As shown in Figure 8(a) and (b), the phonon lifetime under electric field of  $0.04 \text{ V/\AA}$  is obviously longer than that for the other two cases of electric fields, especially in the low frequency range (7.5-10 THz). This variation trend of the lifetime is consistent with the lattice thermal conductivity of borophene with different electric fields, which means that phonon lifetime is the dominant factor for the dramatic change in lattice thermal conductivity as shown in Figure 5(a). In addition, the unexpectedly low lattice thermal conductivity of borophene at large electric field of  $0.4 \text{ V/\AA}$  is mainly attributed to the suppressed phonon lifetime. The lifetime of borophene is generally below 100 ps, which is at least 4 orders of magnitude smaller than that of graphene's dominant ZA modes<sup>36-37</sup>. We further compared the lifetime of three acoustic branches at electric field of  $0.04 \text{ V/\AA}$  in Figure 8(b). The lifetime of LA and TA branches are generally longer than that of ZA in the frequency range of 7.5-10 THz and the group velocities of LA and TA branches are also higher, so the LA and TA branches are the main contributors for lattice thermal conductivity of borophene. In fact, we found that with electric field  $0.04 \text{ V/\AA}$  the contribution of LA and TA branches to overall thermal conductivity of borophene along  $\vec{a}$  and  $\vec{b}$  direction is 75.54% and 56.875%, respectively, which is obviously higher than the other acoustic branch and optical branches (below 30% for each).

For further insight into the anharmonic interactions, the scattering strength and the number of available phonon scattering channels are considered, which are characterized by the phase space<sup>38</sup> and the Grüneisen parameter<sup>39</sup>. Owing to the little differences in the phonon dispersion, the phase space of borophene changes slightly under the different electric fields. The Grüneisen parameters are depicted in Figure 8(c), we found that the magnitude of the Grüneisen parameter is decreased greatly when the electric field of  $0.4 \text{ V/\AA}$  is applied. In contrast, the Grüneisen parameter under both electric fields ( $0 \text{ V/\AA}$  and  $0.04 \text{ V/\AA}$ ) are higher apparently. Furthermore, the average Grüneisen parameters of borophene under electric fields of  $0 \text{ V/\AA}$ ,  $0.04 \text{ V/\AA}$ , and  $0.4 \text{ V/\AA}$  are 0.476, 0.125, and -8.649, respectively. It is known that the larger the absolute value of Grüneisen parameter, the stronger the anharmonicity. The lower absolute value of Grüneisen parameter under the electric field of  $0.04 \text{ V/\AA}$  leads to higher thermal conductivity. Thus, the change of the phonon anharmonicity is the underlying mechanism for the variation of the phonon lifetime and further thermal conductivity of borophene variation upon applying an electric field.

The phonon anharmonic behavior can be traced back to the response of atom and structure distortion. In order to have an intuitive understanding of the phonon anharmonicity, the potential well is depicted in Figure 8(d). The potential well changes in a symmetric way when the boron atom vibrates around its equilibrium position along the  $\vec{a}$  and  $\vec{b}$  direction, while it changes in an asymmetric way for the out-of-plane directions [see Figure 8(d)]. It is found that the potential well becomes flatter with stronger electric fields applied when boron oscillating along the out-of-plane direction, indicating more asymmetry and the nonlinear dependence of restoring forces on atomic displacement amplitudes<sup>40-41</sup>. In the meantime, the average Grüneisen parameter of the ZA branch under the electric field of  $0 \text{ V/\AA}$ ,  $0.04 \text{ V/\AA}$ , and  $0.4 \text{ V/\AA}$  are calculated, the results are -1.653, -4.041, and -27.737 respectively, which are consistent with the trend of potential well under the electric field affection.

So far, the reason for the sudden increase in the anisotropy of borophene thermal conductivity at electric field of  $0.04 \text{ V/\AA}$  has been identified. The intrinsic structure of borophene makes the phonon group velocity differ along the  $\vec{a}$  and  $\vec{b}$  direction, but this difference is relatively constant at different electric fields. According to Eq. (1), the lattice thermal conductivity is the product of the three terms, namely specific heat capacity, group velocity, and phonon lifetime. Therefore, it is understandable that the phonon

lifetime is an amplifying factor of the difference in the group velocity. Among all the representative electric fields, the phonon lifetime of borophene is enhanced obviously by applying electric field of  $0.04 \text{ V}/\text{\AA}$ . Especially, in the frequency region of 7.5-10THz the phonon lifetime of LA and TA branches are significantly improved compared to ZA branch, which amplifies the difference in the anisotropy of group velocity. Therefore, not only the thermal conductivity value itself increases steeply at the electric field of  $0.04 \text{ V}/\text{\AA}$ , but also the anisotropy of the thermal conductivity is dramatically enhanced [see Figure 6]. It is worth pointing out that, among all the methods for regulating physical properties of materials, the external electric field acts relatively mildly, which not only has a negligible impact on the atomic structure of the material, but also is reversible and thus the effect can go back and forth.

### 3.5 Insight from electronic structures

As mentioned above, the effect of electric field on the value and anisotropy of borophene thermal conductivity are attribute to the phonon anharmonicity. Considering the inherent relationship between the phonon transport characteristics and interatomic electrostatic interaction, we will explore the underlying mechanism responsible for the electric field regulated phonon transport characteristics and phonon anharmonicity from the perspective of electronic structure. The electron localization function (ELF) has already been used to characterize the interatomic bonding in lots of previous studies<sup>42-43-44-45</sup>. To understand the bonding characteristics in borophene, the ELF is calculated and the result is shown in Figure 9. The ELF is a position dependent function with values that range from 0 to 1.  $\text{ELF} = 1$  corresponds to perfect localization,  $\text{ELF} = 0.5$  corresponds to the electron-gas like pair probability, and  $\text{ELF} = 0$  corresponds to the electrons fully delocalized or electroless state. Figure 9(a) is the top view of 3D ELF of borophene, where  $B_1$  and  $B_2$  are the upper and lower boron atoms, respectively. From Figure 9(b) and (c) it is easily seen that the electrons are accumulated on top of the upper plane and the bottom of the lower plane, indicating the atomic orbitals of borophene contain more  $sp^3$  hybridization. The  $sp^3$  hybridization induces the buckled structure which stabilizes the whole crystal structure. Figure 9(d) is the ELF profile of borophene viewed along the (110) direction. The electronic charges are localized near  $B_1$  and  $B_2$  bonds, indicating strong covalent bonding between  $B_1$  and  $B_2$  atoms.

For the electric field of  $0.4 \text{ V/\AA}$  that significantly reduces the phonon lifetime and anisotropy, we explain it from the electronic structure. The dielectric constant is a common physical concept in dielectric physics. It reflects the ability of charge in the material to be polarized under an applied electric field, thereby screening the external field, which is a crucial factor for carrier transport. Figure 10(a) is the dielectric constant of borophene with respect to the external electric field. With a small electric field applied ( $<0.02 \text{ V/\AA}$ ), the orientation of charge keeps in random, making the dielectric constant very slight. When the external electric field is bigger than that of  $0.02 \text{ V/\AA}$ , it will polarize the charge by orienting the dipole moments, the positive accumulation of charge and negative depletion of charges caused by the electric field leads to induced charges with opposite signs, which are located around the boron cores [see Figure 10(c)]. The dielectric constant curve first increases until the external electric field reaches  $0.04 \text{ V/\AA}$ , and then begins to decrease. By comparing the electric field-modulated thermal conductivity of borophene [see Figure 5(a)] with the dielectric constant, it is found that the variation trend of thermal conductivity is similar to that of dielectric constant, which can be understood in terms of charge accumulation or depletion<sup>46</sup>. In order to study the effect of the electric field on the borophene charge environment, the charge density distribution under each electric field is subtracted by the charge density distribution without electric field. Figure 10(b) is the difference of charge density along the extracting path illustrated in the inset. It is found that the stronger the electric field, the more induced charges there are, the screening effect will be stronger, therefore the dielectric constant will increase as the electric field increases ( $<0.04 \text{ V/\AA}$ ). However, if the external electric field continues to increase ( $>0.04 \text{ V/\AA}$ ), although more induced charges are generated, the induced charges are repelled away from the boron core by external electric field, the dielectric constant decreases. This may be due to the ability of charge redistribution in the electric field is limited<sup>46</sup> or the polarizable charge is saturated<sup>47</sup>. Therefore, the charge environment between boron atoms are renormalized by the electric field which will lead to phonon renormalization and modulation of phonon anharmonicity<sup>48-</sup>

49-50-51

In addition, positive accumulation of charge appears in the negative range of boron atoms, the negative depletion of charge should appear in the positive range of boron atom, but more charge is accumulated in this range, because of interaction between  $B_1$ - $B_2$  atoms, which will affect the anisotropic character. Figure

10(c) and (d) are the difference of charge density of borophene under electric field  $0.2 \text{ V/\AA}$  and  $0.4 \text{ V/\AA}$ , respectively. It can be seen in Figure 10(c) that the difference of electron density distribution is dense and continuous along the  $B_1$ – $B_1$  chain ( $\vec{b}$  direction), while there are obvious gaps (discontinuous) between the chains along the  $\vec{a}$  direction, which is the root reason for the anisotropy of thermal conductivity (group velocity in  $\vec{b}$  direction is higher than that in  $\vec{a}$  direction) [see Figure 5(a)]. However, under the electric field of  $0.4 \text{ V/\AA}$ , the difference of charge density exists along both  $\vec{a}$  and  $\vec{b}$  directions [see Figure 10(d)], which reduces the anisotropy of thermal conductivity. Although it is challenging to quantitatively describe the behavior of ELF and difference of electric distribution, the above analysis evidently shows the variation of the charge environment felt by the boron cores, which renormalizes the interactions between boron atoms and is believed to have a consequent influence on the phonon anharmonicity and further the anisotropy of thermal conductivity.

#### 4 Conclusion

In summary, first-principles calculations combined with phonon BTE are performed to systematically investigate the effect of external electric field on the thermal transport of monolayer borophene. At room temperature the thermal conductivities of borophene first dramatically increase and then steeply drop with the strength of electric field increasing. More interestingly, the intrinsic anisotropy of the thermal conductivity first increases to the peak value of 2.13 at electric field of  $0.04 \text{ V/\AA}$ . As the strength of electric field increases, the anisotropy of the thermal conductivity decreases and exhibits an oscillating behavior. The thermal transport in borophene finally transits into isotropic regime when the strength of electric field is increased to  $0.4 \text{ V/\AA}$ , i.e. the thermal conductivities in the two in-plane directions are almost equal despite of the intrinsic anisotropic structure of borophene. The analysis of phonon related properties reveals that, due to the anisotropic structure, the difference in the phonon group velocity along  $\vec{a}$  and  $\vec{b}$  direction is the root reason for the intrinsic anisotropy of thermal conductivity of borophene. With moderate external electric field of  $0.04 \text{ V/\AA}$  applied, the phonon lifetime acts as an amplifying factor and thus the anisotropy of thermal conductivity of borophene is substantially enlarged. At highest strength of electric field of  $0.4 \text{ V/\AA}$ , the phonon lifetime is extremely suppressed and eliminates the intrinsic difference in the phonon

group velocity along  $\vec{a}$  and  $\vec{b}$  direction, resulting in isotropic thermal transport in borophene. The underlying mechanism is further understood in terms of the bonding characteristics and electron localization function. With an electric field applied, due to the screened potential resulting from the ability of charge redistribution, the interactions between boron atoms are renormalized, which leads to phonon renormalization and the modulation of phonon anharmonicity. Consequently, the thermal conductivity and anisotropy are drastically enhanced or reduced by the external electric field. The results gained from this work unveil a general relation between thermal transport and electric field for low-dimensional materials, which provide important guidance for designing nanomaterials with desirable thermal transport properties for specific energy applications.

## **Acknowledgement**

This project is supported by the PhD start-up fund of Natural Science Foundation of Liaoning Province, China (Grant No. 20180540122, 200005636, 200005720). Z. Y. gratefully acknowledges Dr Guangzhao Qin (Hunan University) and Dr Yufei Gao (Dalian University of Technology) for their helpful and fruitful discussions. K.Y. acknowledges the support from the China Scholarship Council. Research reported in this publication was supported in part by the NSF (award number 1905775) and SC EPSCoR/IDeA Program under NSF OIA-1655740 via SC EPSCoR/IDeA 20-SA05.

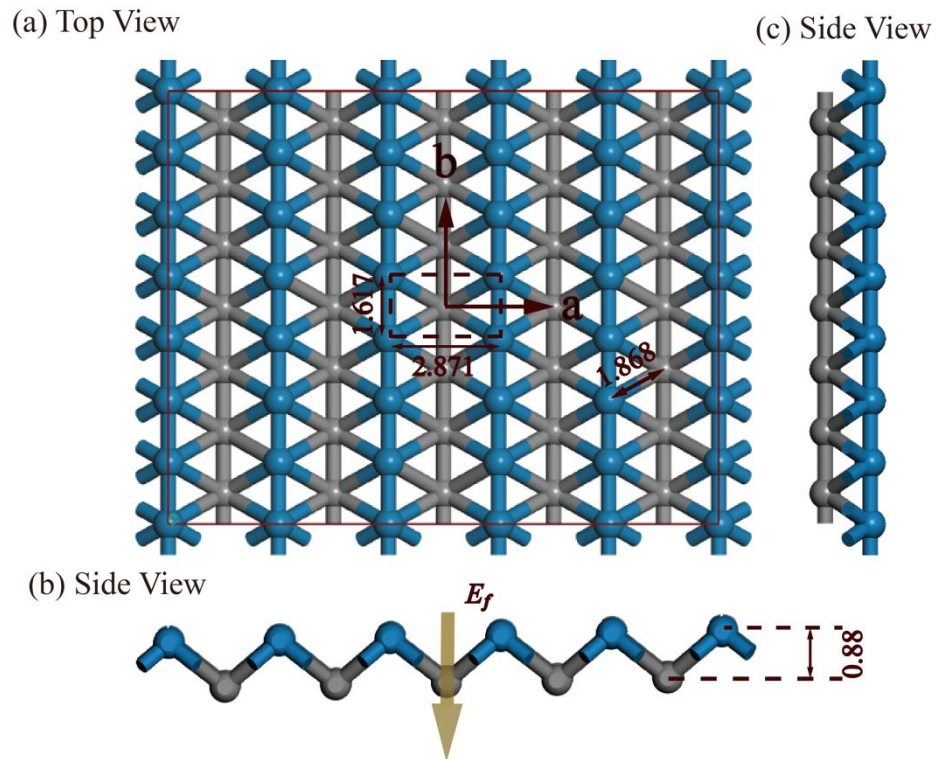
## Reference

1. Piazza, Z. A.; Hu, H.-S.; Li, W.-L.; Zhao, Y.-F.; Li, J.; Wang, L.-S., Planar hexagonal B36 as a potential basis for extended single-atom layer boron sheets. *Nature Communications* **2014**, *5* (1), 3113.
2. Mannix, A. J.; Zhou, X.-F.; Kiraly, B.; Wood, J. D.; Alducin, D.; Myers, B. D.; Liu, X.; Fisher, B. L.; Santiago, U.; Guest, J. R.; Yacaman, M. J.; Ponce, A.; Oganov, A. R.; Hersam, M. C.; Guisinger, N. P., Synthesis of borophenes: Anisotropic, two-dimensional boron polymorphs. *Science* **2015**, *350* (6267), 1513.
3. Lopez-Bezanilla, A.; Littlewood, P. B., Electronic properties of 8–Pmmn borophene. *Physical Review B* **2016**, *93* (24), 241405.
4. Wang, V.; Geng, W. T., Lattice Defects and the Mechanical Anisotropy of Borophene. *The Journal of Physical Chemistry C* **2017**, *121* (18), 10224-10232.
5. Liu, X.; Zhang, Z.; Wang, L.; Yakobson, B. I.; Hersam, M. C., Intermixing and periodic self-assembly of borophene line defects. *Nature Materials* **2018**, *17* (9), 783-788.
6. Cui, H.; Zhang, X.; Chen, D., Borophene: a promising adsorbent material with strong ability and capacity for SO<sub>2</sub> adsorption. *Applied Physics A* **2018**, *124* (9).
7. Wang, Z.-Q.; Lü, T.-Y.; Wang, H.-Q.; Feng, Y. P.; Zheng, J.-C., Review of borophene and its potential applications. *Frontiers of Physics* **2019**, *14* (3), 33403.
8. Li, D.; Chen, Y.; He, J.; Tang, Q.; Zhong, C.; Ding, G., Review of thermal transport and electronic properties of borophene. *Chinese Physics B* **2018**, *27* (3), 036303.
9. Zhou, H.; Cai, Y.; Zhang, G.; Zhang, Y.-W., Superior lattice thermal conductance of single-layer borophene. *npj 2D Materials and Applications* **2017**, *1* (1), 14.
10. Peng, B.; Zhang, H.; Shao, H.; Xu, Y.; Zhang, R.; Zhu, H., The electronic, optical, and thermodynamic properties of borophene from first-principles calculations. *Journal of Materials Chemistry C* **2016**, *4* (16), 3592-3598.
11. Mortazavi, B.; Le, M.-Q.; Rabczuk, T.; Pereira, L. F. C., Anomalous strain effect on the thermal conductivity of borophene: a reactive molecular dynamics study. *Physica E: Low-dimensional Systems and Nanostructures* **2017**, *93*, 202-207.
12. Liu, Y.; Dong, Y.-J.; Tang, Z.; Wang, X.-F.; Wang, L.; Hou, T.; Lin, H.; Li, Y., Stable and metallic borophene nanoribbons from first-principles calculations. *Journal of Materials Chemistry C* **2016**, *4* (26), 6380-6385.
13. Xiao, H.; Cao, W.; Ouyang, T.; Guo, S.; He, C.; Zhong, J., Lattice thermal conductivity of borophene from first principle calculation. *Scientific Reports* **2017**, *7* (1), 45986.
14. Gao, M.; Li, Q.-Z.; Yan, X.-W.; Wang, J., Prediction of phonon-mediated superconductivity in borophene. *Physical Review B* **2017**, *95* (2), 024505.
15. Xiao, R. C.; Shao, D. F.; Lu, W. J.; Lv, H. Y.; Li, J. Y.; Sun, Y. P., Enhanced superconductivity by strain and carrier-doping in borophene: A first principles prediction. *Applied Physics Letters* **2016**, *109* (12), 122604.
16. Wang, H.; Li, Q.; Gao, Y.; Miao, F.; Zhou, X.-F.; Wan, X. G., Strain effects on borophene: ideal strength, negative Poisson's ratio and phonon instability. *New Journal of Physics* **2016**, *18* (7), 073016.
17. Kresse, G.; Furthmüller, J., Efficiency of ab-initio total energy calculations for metals and semiconductors using a plane-wave basis set. *Computational Materials Science* **1996**, *6* (1), 15-50.
18. Kresse, G.; Furthmüller, J., Efficient iterative schemes for ab initio total-energy calculations using a plane-wave basis set. *Physical Review B* **1996**, *54* (16), 11169-11186.
19. Kresse, G.; Joubert, D., From ultrasoft pseudopotentials to the projector augmented-wave method. *Physical*

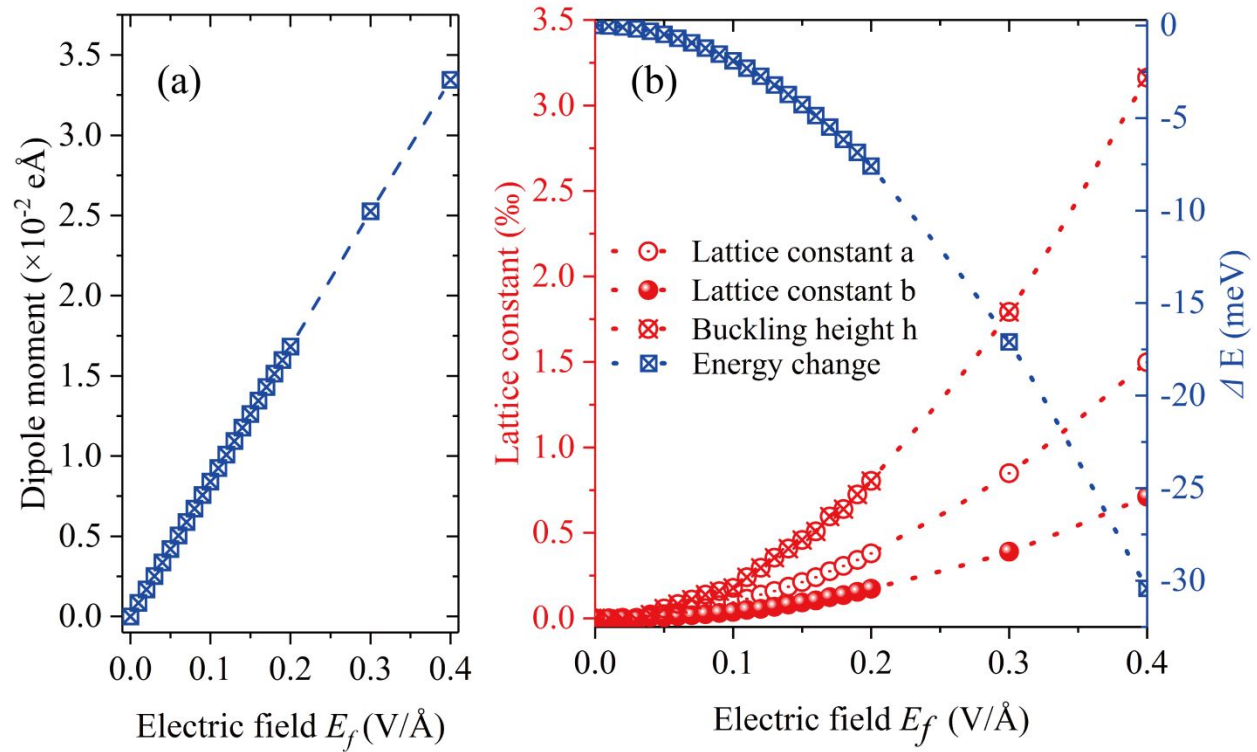
*Review B* **1999**, *59* (3), 1758-1775.

20. Perdew, J. P.; Burke, K.; Ernzerhof, M., Generalized Gradient Approximation Made Simple. *Physical Review Letters* **1996**, *77* (18), 3865-3868.
21. Monkhorst, H. J.; Pack, J. D., Special points for Brillouin-zone integrations. *Physical Review B* **1976**, *13* (12), 5188-5192.
22. Huang, D.; Kaxiras, E., Electric field tuning of band offsets in transition metal dichalcogenides. *Physical Review B* **2016**, *94* (24), 241303.
23. Li, W.; Carrete, J.; A. Katcho, N.; Mingo, N., ShengBTE: A solver of the Boltzmann transport equation for phonons. *Computer Physics Communications* **2014**, *185* (6), 1747-1758.
24. Togo, A.; Oba, F.; Tanaka, I., First-principles calculations of the ferroelastic transition between rutile-type and CaCl<sub>2</sub>-type SiO<sub>2</sub> at high pressures. *Physical Review B* **2008**, *78* (13), 134106.
25. Yuan, J.; Zhang, L. W.; Liew, K. M., Effect of grafted amine groups on in-plane tensile properties and high temperature structural stability of borophene nanoribbons. *RSC Advances* **2015**, *5* (91), 74399-74407.
26. Qin, G.; Qin, Z.; Wang, H.; Hu, M., On the diversity in the thermal transport properties of graphene: A first-principles-benchmark study testing different exchange-correlation functionals. *Computational Materials Science* **2018**, *151*, 153-159.
27. Lee, S.; Esfarjani, K.; Luo, T.; Zhou, J.; Tian, Z.; Chen, G., Resonant bonding leads to low lattice thermal conductivity. *Nature Communications* **2014**, *5* (1), 3525.
28. Sun, H.; Li, Q.; Wan, X., First-Principles Study of Thermal Properties of Borophene. *Phys. Chem. Chem. Phys.* **2016**, *18*.
29. Qin, G.; Qin, Z.; Fang, W.-Z.; Zhang, L.-C.; Yue, S.-Y.; Yan, Q.-B.; Hu, M.; Su, G., Diverse anisotropy of phonon transport in two-dimensional group IV–VI compounds: A comparative study. *Nanoscale* **2016**, *8* (21), 11306-11319.
30. Qin, G.; Yan, Q.-B.; Qin, Z.; Yue, S.; Hu, M.; Su, G., Anisotropic Intrinsic Lattice Thermal Conductivity of Phosphorene from First Principles. *Phys. Chem. Chem. Phys.* **2014**, *17*, 4854-4858.
31. Xie, H.; Hu, M.; Bao, H., Thermal conductivity of silicene from first-principles. *Applied Physics Letters* **2014**, *104* (13), 131906.
32. Gu, X.; Yang, R., First-principles prediction of phononic thermal conductivity of silicene: A comparison with graphene. *Journal of Applied Physics* **2015**, *117* (2), 025102.
33. Morelli, D. T.; Heremans, J. P., Thermal conductivity of germanium, silicon, and carbon nitrides. *Applied Physics Letters* **2002**, *81* (27), 5126-5128.
34. Jain, A.; McGaughey, A. J. H., Strongly anisotropic in-plane thermal transport in single-layer black phosphorene. *Scientific reports* **2015**, *5*, 8501-8501.
35. Efetov, D. K.; Kim, P., Controlling Electron-Phonon Interactions in Graphene at Ultrahigh Carrier Densities. *Physical Review Letters* **2010**, *105* (25), 256805.
36. Lindsay, L.; Li, W.; Carrete, J.; Mingo, N.; Broido, D. A.; Reinecke, T. L., Phonon thermal transport in strained and unstrained graphene from first principles. *Physical Review B* **2014**, *89* (15), 155426.
37. Kuang, Y.; Lindsay, L.; Shi, S.; Wang, X.; Huang, B., Thermal conductivity of graphene mediated by strain and size. *International Journal of Heat and Mass Transfer* **2016**, *101*, 772-778.
38. Manley, M. E.; Hellman, O.; Shulumba, N.; May, A. F.; Stonaha, P. J.; Lynn, J. W.; Garlea, V. O.; Alatas, A.; Hermann, R. P.; Budai, J. D.; Wang, H.; Sales, B. C.; Minnich, A. J., Intrinsic anharmonic localization in

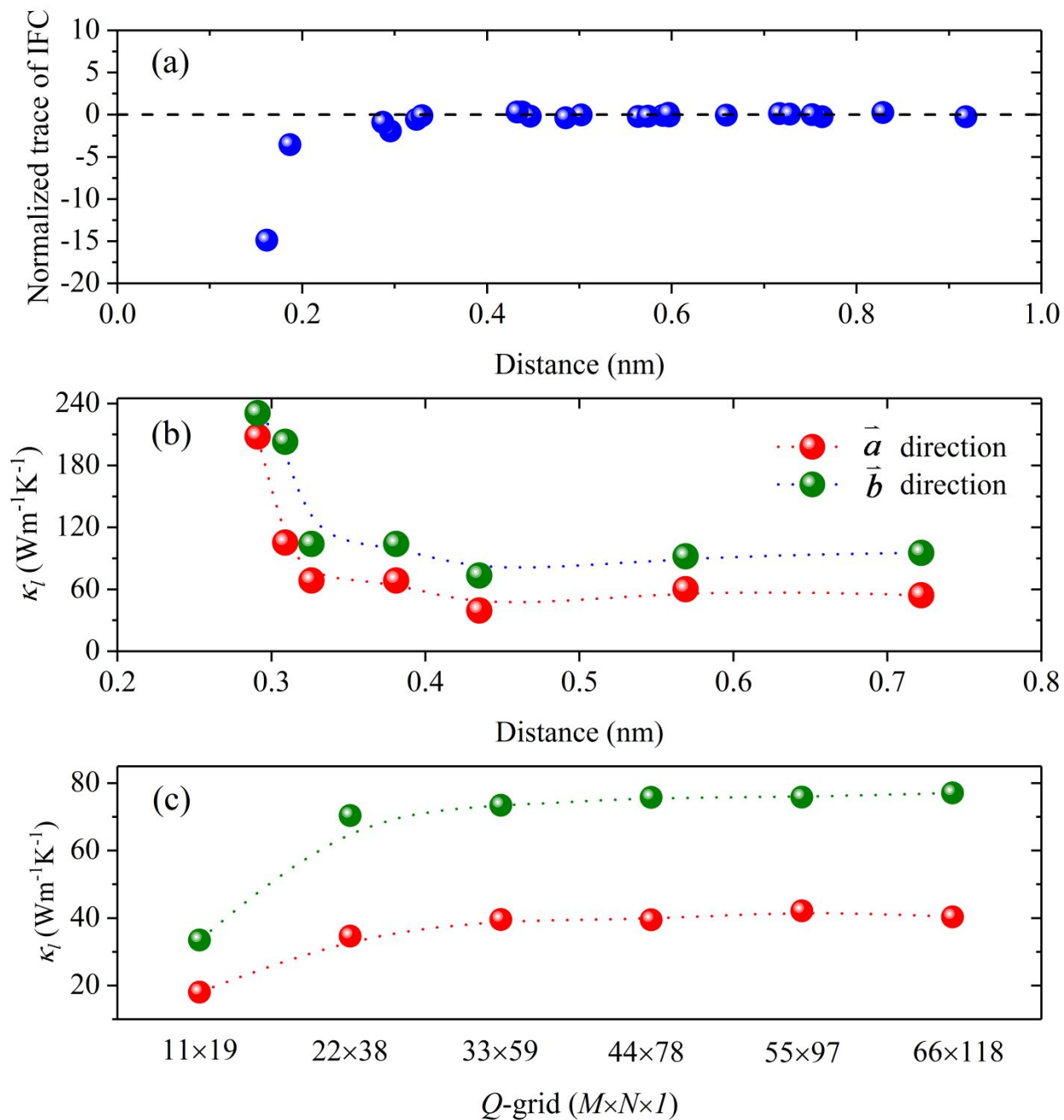
- thermoelectric PbSe. *Nature Communications* **2019**, *10* (1), 1928.
39. Zhang, S.; Xu, B.; Lin, Y.; Nan, C.; Liu, W., First-principles study of the layered thermoelectric material TiNBr. *RSC Advances* **2019**, *9* (23), 12886-12894.
40. Zhao, L.-D.; Chang, C.; Tan, G.; Kanatzidis, M. G., SnSe: a remarkable new thermoelectric material. *Energy & Environmental Science* **2016**, *9* (10), 3044-3060.
41. Zeier, W. G.; Zevalkink, A.; Gibbs, Z. M.; Hautier, G.; Kanatzidis, M. G.; Snyder, G. J., Thinking Like a Chemist: Intuition in Thermoelectric Materials. *Angewandte Chemie International Edition* **2016**, *55* (24), 6826-6841.
42. Ouyang, T.; Hu, M., Competing mechanism driving diverse pressure dependence of thermal conductivity of  $XTe$  ( $X=Hg, Cd, \text{ and } Zn$ ). *Physical Review B* **2015**, *92* (23), 235204.
43. Qin, G.; Qin, Z.; Wang, H.; Hu, M., Lone-pair electrons induced anomalous enhancement of thermal transport in strained planar two-dimensional materials. *Nano Energy* **2018**, *50*, 425-430.
44. Qin, G.; Zhang, X.; Yue, S.-Y.; Qin, Z.; Wang, H.; Han, Y.; Hu, M., Resonant bonding driven giant phonon anharmonicity and low thermal conductivity of phosphorene. *Physical Review B* **2016**, *94* (16), 165445.
45. Qin, G.; Qin, Z.; Wang, H.; Hu, M., Anomalously temperature-dependent thermal conductivity of monolayer GaN with large deviations from the traditional  $1/T$  law. *Physical Review B* **2017**, *95* (19), 195416.
46. Qin, G.; Qin, Z.; Yue, S.; Yan, Q.-B.; Hu, M., External electric field driving the ultra-low thermal conductivity of silicene. *Nanoscale* **2017**, *9*.
47. Furukawa, T.; Nakajima, K.; Koizumi, T.; Date, M., Measurements of Nonlinear Dielectricity in Ferroelectric Polymers. *Japanese Journal of Applied Physics* **1987**, *26* (Part 1, No. 7), 1039-1045.
48. Liao, B.; Qiu, B.; Zhou, J.; Huberman, S.; Esfarjani, K.; Chen, G., Significant Reduction of Lattice Thermal Conductivity by the Electron-Phonon Interaction in Silicon with High Carrier Concentrations: A First-Principles Study. *Physical Review Letters* **2015**, *114* (11), 115901.
49. Zhuang, J.; Xu, X.; Du, Y.; Wu, K.; Chen, L.; Hao, W.; Wang, J.; Yeoh, W. K.; Wang, X.; Dou, S. X., Investigation of electron-phonon coupling in epitaxial silicene by in situ Raman spectroscopy. *Physical Review B* **2015**, *91* (16), 161409.
50. Zhang, P.; Louie, S. G.; Cohen, M. L., Nonlocal Screening, Electron-Phonon Coupling, and Phonon Renormalization in Metals. *Physical Review Letters* **2005**, *94* (22), 225502.
51. Yan, J.-A.; Stein, R.; Schaefer, D. M.; Wang, X.-Q.; Chou, M. Y., Electron-phonon coupling in two-dimensional silicene and germanene. *Physical Review B* **2013**, *88* (12), 121403.



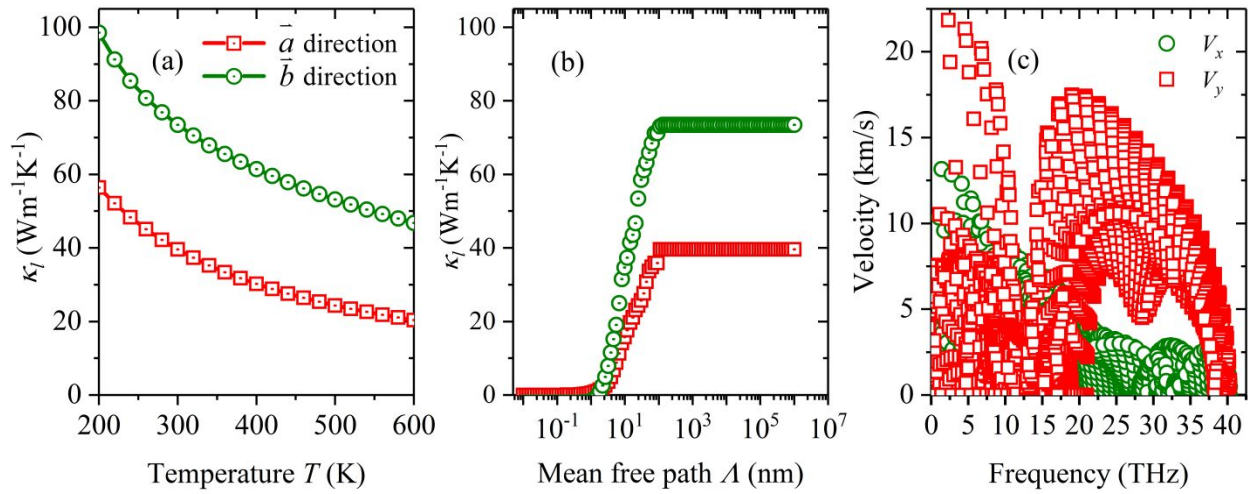
**Figure 1.** The atom structure of borophene in (a) top and (b) side views. The two in-plane directions ( $\vec{a}$  and  $\vec{b}$ ) are defined in the top panel. Atoms in different planes are distinguished by different colors (blue and gray) with a buckling distance of 0.88 Å. The primitive cells are shown by dashed lines. The electric field is applied along the downward out-of-plane direction as indicated by the arrow in the bottom panel.



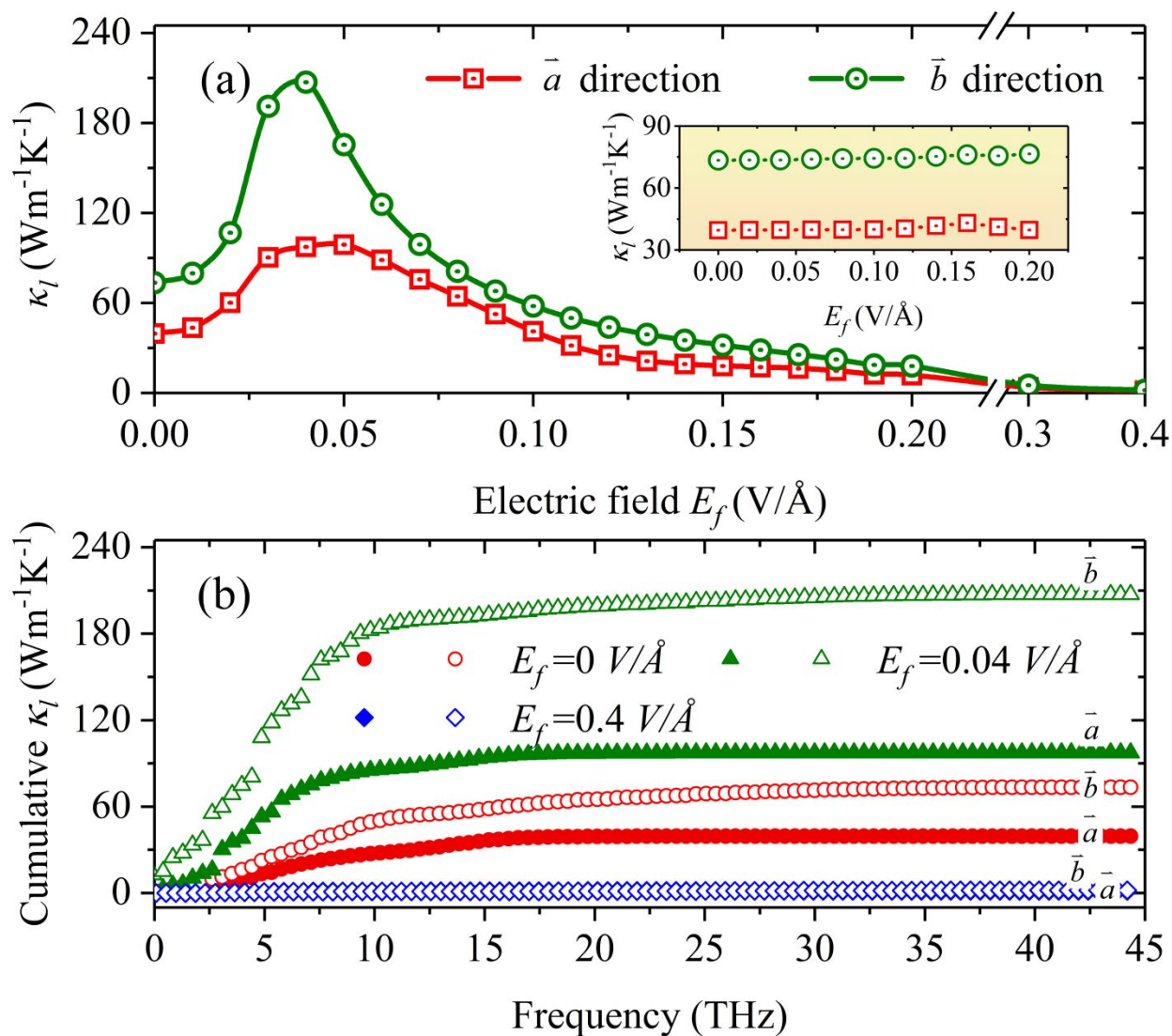
**Figure 2.** (a) The dipole moment and (b) The changes of atom structure (left-axis) and energy (right-axis) as a function of the strength of external electric field.



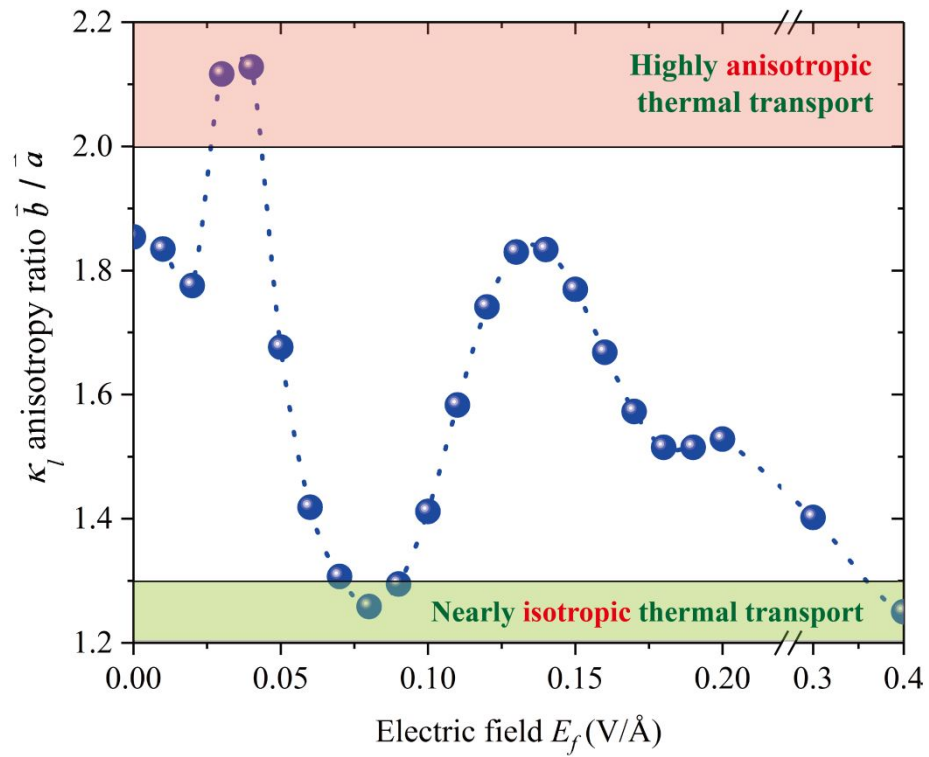
**Figure 3.** (a) Normalized trace of interatomic force constant tensors versus atomic distances. (b) Convergence test of thermal conductivity with respect to cutoff radius. (c) Convergence test of thermal conductivity with respect to  $Q$ -grid.



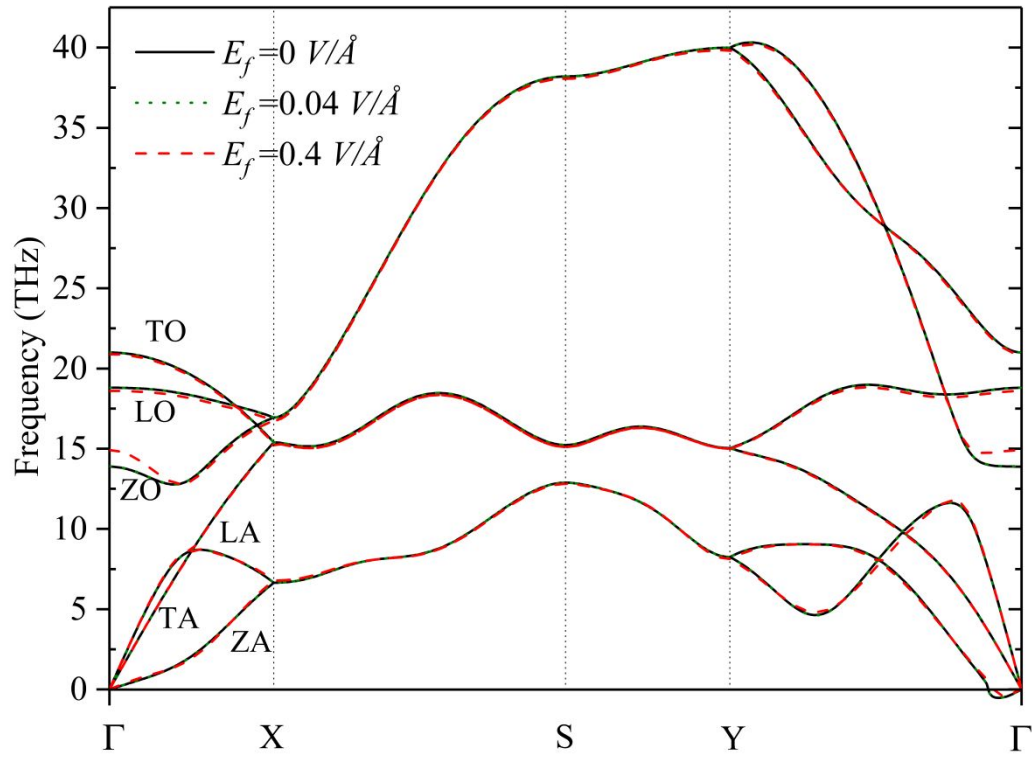
**Figure 4.** (a) The temperature dependent lattice thermal conductivity along  $a$ - and  $b$ -axis. (b) The mean free path dependent cumulative lattice thermal conductivity  $a$ - and  $b$ -axis. (c) Comparison of frequency dependent phonon group velocities in the two in-plane directions ( $\vec{a}$  and  $\vec{b}$ ).



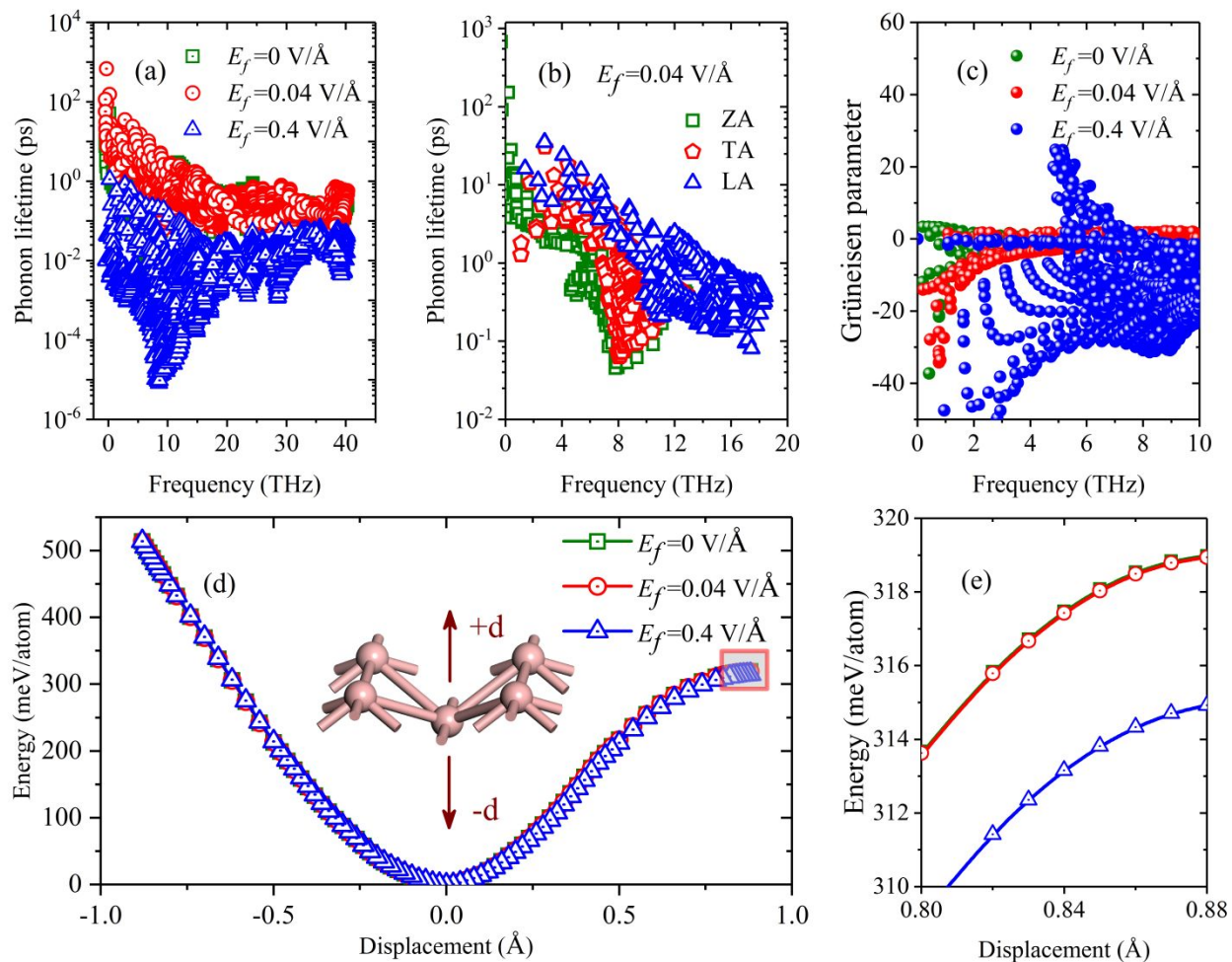
**Figure 5.** (a) Lattice thermal conductivity of borophene at 300 K with different strength of external electric field. (Inset) the effect of atom structure on lattice thermal conductivity. The abscissa represents the atomic structure of different electric field (0 – 0.2 V/Å). (b) The frequency dependent cumulative thermal conductivity of borophene at 300 K with different strengths of external electric field.



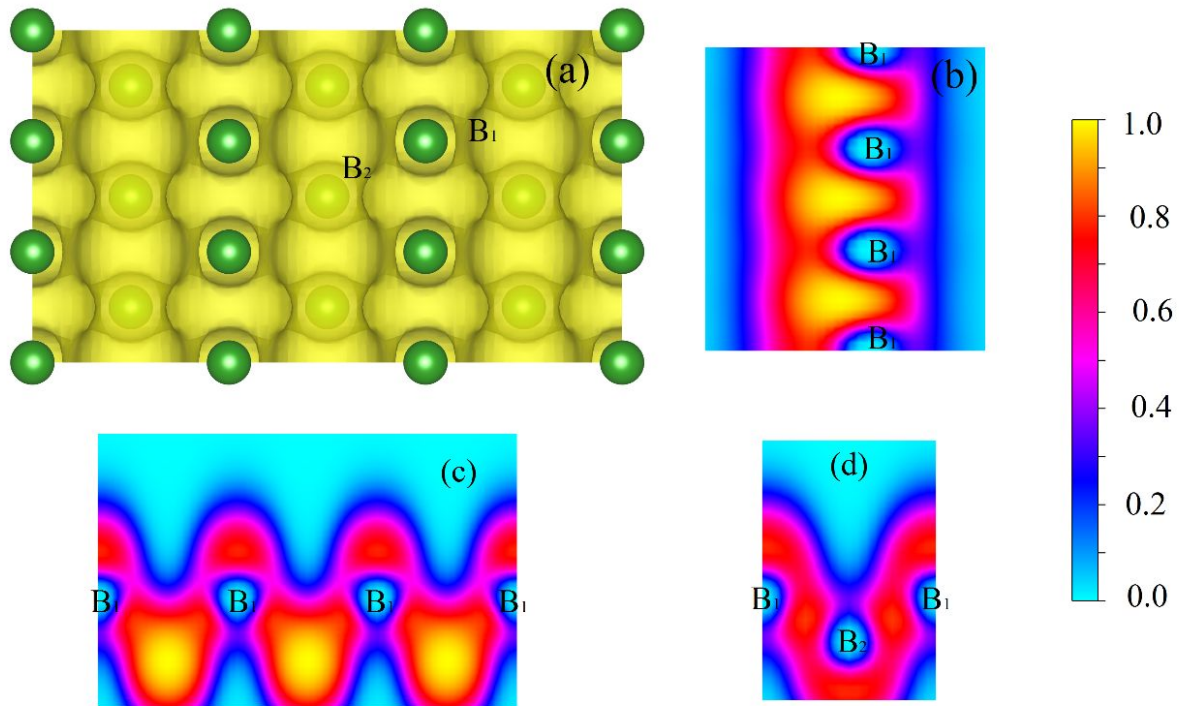
**Figure 6.** Anisotropy ratio of borophene at room temperature as a function of the strength of external electric field. The upper and lower shaded area denotes the highly anisotropic and nearly isotropic thermal transport, respectively.



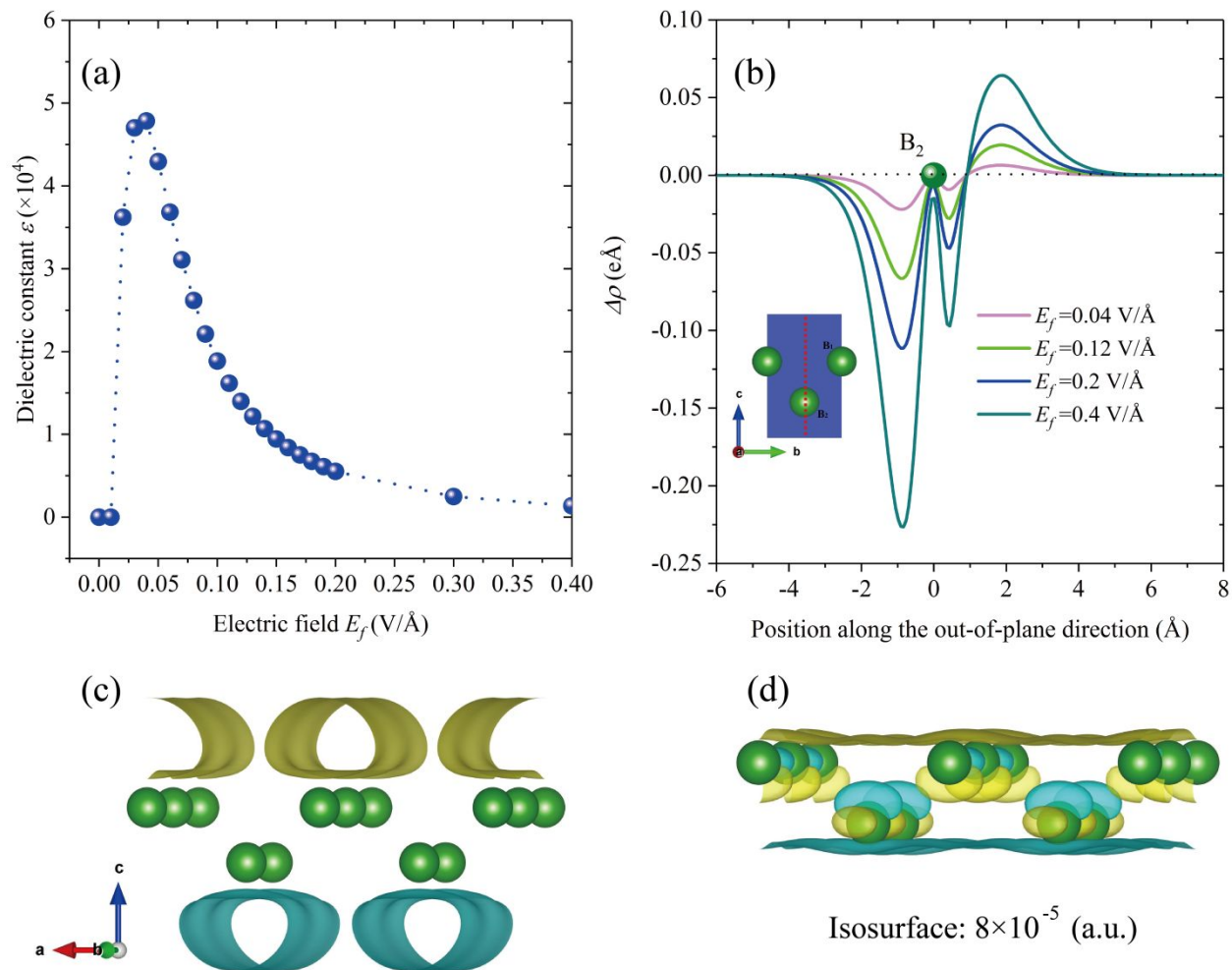
**Figure 7.** Phonon dispersion of borophene under representative electric fields with phonon polarization labeled.



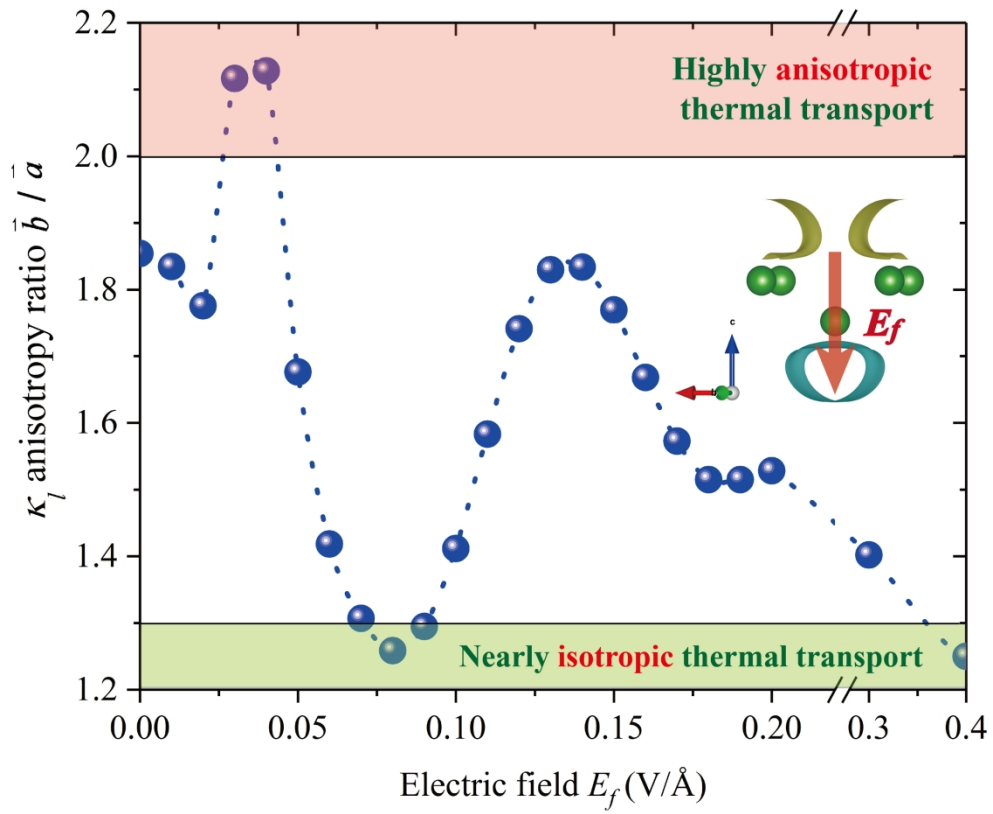
**Figure 8.** (a) The phonon lifetime under representative electric fields. (b) Comparison of the phonon lifetime of three acoustic branches at electric field of  $0.04$  V/Å. (c) The Grüneisen parameter of borophene under representative electric fields. (d) The potential energy change per atom with respect to displacement of boron atom along the out-of-plane direction. (e) Zoom-in of the potential energy change near the displacement of  $0.80$  Å.



**Figure 9.** The view of 3D ELF and 2D electron localization function (ELF) profiles of borophene. (a) Top view (isosurface value = 0.6), side view along (b) (100), (c) (010), and (d) (110) direction.



**Figure 10.** (a) The dielectric constant as a function of the strength of external electric field. (b) The difference of charge density caused by the electric field ( $\Delta\rho = \rho(E_f) - \rho(E_f = 0)$ ). Comparison of the difference of charge density distribution along the vertical path as shown in the inset (red dashed line). (c) The borophene difference of charge density under electric field of  $0.04 V/\text{\AA}$ , the  $\vec{a}$  and  $\vec{b}$  directions are labeled. (yellow: positive accumulation of charge, blue: negative depletion of charge). (d) The borophene difference of charge density under electric field of  $0.4 V/\text{\AA}$ , the isosurface is set as  $8 \times 10^{-5}$  (a.u.).



224x183mm (300 x 300 DPI)